



Full paper

Self-driven power management system for triboelectric nanogenerators

William Harmon^a, David Bamgboje^a, Hengyu Guo^b, Tingshu Hu^{a,*}, Zhong Lin Wang^b

^a Department of Electrical and Computer Engineering, University of Massachusetts Lowell, 1 University Avenue, Lowell, MA, 01854, USA

^b School of Materials Science & Engineering, Georgia Institute of Technology, Atlanta, GA, 30332, USA



ARTICLE INFO

Keywords:

Self-powered system
Triboelectric nanogenerator
Power management
Power electronics

ABSTRACT

This paper presents a fully functional power management system for triboelectric nanogenerators (TENGs) with the TENG as the only power source. TENG was developed for the objective to provide power to electronic devices and sensors without the need for a battery (the so-called self-powered systems). A unique feature of the TENG's electrical output is high pulsed voltage but low current capability, making TENGs unsuitable for direct use as a power source. To provide continuous and steady electrical voltage for conventional electronics, a power management system (PMS) is required. Existing PMS' based on power electronic converters do not provide a complete solution due to the use of additional power sources for the logic circuit and switch drivers. The PMS to be reported in this work provides a complete solution for a self-powered system with the TENG as the only power source. This goal is accomplished with a novel approach of employing discrete semiconductor devices, including a silicon-controlled rectifier (SCR) and zener diodes, for controlling the power flow paths, without using any integrated circuit. The effectiveness of the newly developed PMS has been experimentally validated with a prototype and a contact and separation mode TENG device.

1. Introduction

Harvesting irregular ambient energy from daily activities, such as walking and exercising, and using it to power mobile electronic devices, IoT devices, and health monitors, is becoming a reality with the development of nanogenerators such as piezoelectric, triboelectric, and thermoelectric nanogenerators (Fig. 1a), which convert kinetic or thermal energy into electricity using nano-structures [1–3]. As compared with traditional energy harvesters, these nanogenerators are small, wearable, and can operate at anytime, anywhere, regardless of weather conditions. They can be used to provide supplementary energy to extend the battery life or as independent power sources. The ultimate goal is to resolve some energy and environmental issues by eliminating the need for batteries with self-powered electronic devices, and to generate sustainable energy.

Of these nanogenerators, TENG is the most recent technology which was first proposed by Zhong Lin Wang in 2012 and subsequently reported in [2,4,5]. The TENGs are also called organic nanogenerators since the most useful materials are organic and can be very cheap and easy to manufacture [6]. Other appealing advantages of TENGs include high voltage output, high power density, stability, robustness, reliability, the simple structure, and environmental friendliness [7–9]. The

past few years have witnessed tremendous advancement of TENG technology with the increase of output power density and conversion efficiency [10,11]. Meanwhile, flexible and stretchable TENGs have been developed for the comfort of wearable devices and sensors [12–14]. To a greater scale, the potential of TENGs for harvesting wind energy [15] and blue energy from the ocean [16–18], has been explored for sustainable energy.

All electrical energy harvested with nanogenerators requires a power management system (PMS) to regulate the random irregular energy to well behaved form which is suitable for electronic devices. Since the invention of TENG, many different PMS' have been developed. Although these PMS' are vastly different, they have a common component, a switch, which can be implemented mechanically or electronically. The idea of using passive mechanical switch for TENG power management can be traced back to Ref. [19], where an off-on-off contact based switch enables instantaneous discharging. In Ref. [20], Zi et al. developed an inductor-free PMS by changing the connections of capacitors with switches driven by a linear motor. Other PMSs utilizing passive mechanical switches have been developed for different types of TENGs, such as the TENG with a unidirectional switch in Ref. [21], TENGs with an electrostatic vibration switch in Refs. [22,23], a sliding mode TENG with an air discharge switch in Ref. [24].

* Corresponding author.

E-mail address: tingshu_hu@uml.edu (T. Hu).

<https://doi.org/10.1016/j.nanoen.2020.104642>

Received 31 January 2020; Received in revised form 17 February 2020; Accepted 20 February 2020

Available online 26 February 2020

2211-2855/© 2020 Elsevier Ltd. All rights reserved.

Another trend in the PMS development is to employ electronic switches in the form of MOSFETs and utilize a certain type of power converter topology, such as the buck converter topology in Xi et al. [25], and the flyback converter topology in Niu et al. [26,27]. The advantage of using electronic switches is that they are more durable, more reliable and more compact than mechanical switches. However, a main concern about the power converter based PMS is that a MOSFET needs a driver and the control of the switch requires logic circuits, which are integrated circuits requiring a dedicated power supply. This implies that a PMS using MOSFETs would not start working without an additional power supply. Therefore the TENG cannot be used as an independent power source for self-powered applications.

In this work, a novel and effective PMS based on a buck converter will be developed for TENGs, which does not require any additional power supply such as a battery, so that the TENG is the only power source for the PMS and the load. This innovation will be a breakthrough in the development of self-powered mobile devices, IoT devices and sensors. This goal is achieved by employing the unique properties of discrete semiconductor devices, the silicon-controlled rectifier (SCR) and zener diode, to control the power flow for efficient energy transfer from the TENG to energy storage devices, instead of using a MOSFET and logic ICs as in traditional power converters. The simple combination of the SCR and Zener diode is able to control the power flow from the TENG to the load as desired in an ideal framework which extracts maximal energy from TENG with a capacitor and then transfers the energy to the load with high efficiency. The power loss in the circuit elements will be analysed with LTSPICE simulation and strategies for minimizing power loss will be discussed.

2. Development of power management system and principle of operation

2.1. A circuit model for TENG

To develop a fully functional and effective power management system for a TENG, it is necessary to understand its basic electrical properties. A circuit model will be critical for the development of the general concept and circuit topology, as well as for simulation to prove the concept and choosing optimal design parameters.

As established by Niu and Wang in 2015 [28], a TENG can be modeled as a series connection of a voltage source and a capacitor, both time varying functions depending on the TENG mode and specific construction of the TENG (see Fig. 1a,b). For example, the voltage and capacitance for the contact separation mode TENG can be expressed as

$$V_{oc}(t) = \frac{\sigma x(t)}{\epsilon_0}, \quad C_{Teng}(t) = \frac{S\sigma x(t)}{(d_0 + x(t))}$$

where $x(t)$ is the separation distance, S is the area of the metal electrodes, ϵ_0 is the permittivity of free space and σ is the tribo-charge surface density which depends on the construction and material of TENG. Based on these functions, a circuit model can be constructed for TENG to simulate its interaction with other circuit elements.

2.2. A general framework for power transfer in TENG power management system

Due to the capacitive internal impedance of TENG, conventional power management strategies (e.g., Fig. 1c) are not able to extract

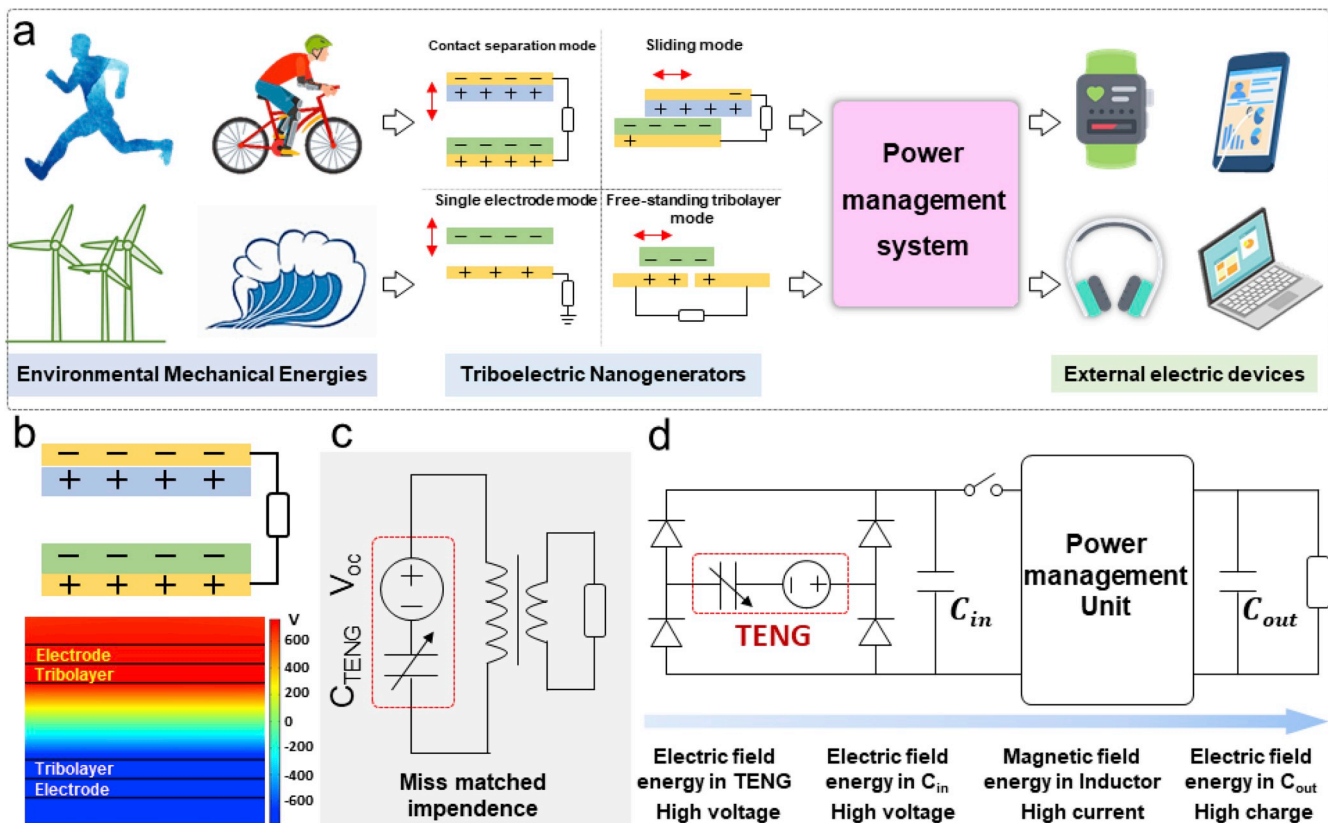


Fig. 1. a) Schematic illustration of a self-powered system using energy harvested with a TENG. A PMS is required to convert the TENG's output with high pulsed voltage and low current into a form suitable for electronic devices.

b) Contact-separation mode TENG's configuration and distribution of voltage potential, demonstrating the TENG's capacitive property and high potential for energy storage.

c) Impedance mismatch between a TENG and a conventional PMS. d) A general framework for TENG power management system.

significant amount of energy from TENG. By the maximum power transfer principle, to draw maximum energy from the TENG, a capacitive load should be used during power transfer, and in practice, a fixed capacitor is used. Since this process takes very brief moment in a TENG charging cycle, a general framework for power management, as illustrated in Fig. 1d, was developed and has been adopted in some literature [25–27].

In Fig. 1d, the TENG is depicted as the series connection of C_{Teng} and V_{oc} inside the box between the diode bridge on the left-hand side. The diode bridge is used to rectify the TENG's bi-directional voltage to a unidirectional voltage. The capacitor C_{in} is the direct load of the TENG to draw the maximum energy during a TENG charge. During the power transfer from the TENG to C_{in} , the power management unit and the load should be disconnected from C_{in} by the switch to ensure an impedance match and maximum power transfer.

The value of C_{in} is selected so that maximum energy is stored in C_{in} after a TENG charge. After the packet of energy is stored in C_{in} , the switch is closed and the PMU transfers the energy from C_{in} to C_{out} and the load. Note that the diode bridge does not allow the energy in C_{in} to be transferred back to the TENG device.

In Niu et al. [26], the PMU is implemented with a flyback converter, where two sequential switches and a transformer are used to first store the energy in the transformer, then transfer it to the load. The two switches are implemented with MOSFETs and controlled by some logic devices. In Xi et al., [25] the PMU is comprised of a buck converter which is implemented with a MOSFET and a comparator.

2.3. A buck converter topology and ideal lossless energy transfer

In this work, the PMS will be derived from the buck converter topology in Fig. 2a. This is different from the buck converter topology in Xi et al. [25], in that the switch SW is to the right of C_{in} while in [25], the switch is between the diode bridge and C_{in} .

In what follows, we address the key design issues for the PMS: 1) the control of the switch's turn on and turn off; 2) Practical and effective implementation of the switch with discrete solid-state devices.

Initially, the switch is off before a TENG charge. During a TENG charge, the voltage across C_{in} increases as energy is stored in it. The switch is triggered to close once the voltage across C_{in} exceeds a threshold value V_T . After the switch is closed, the current flows from C_{in} to the inductor and the load until C_{in} is completely discharged with $V_{Cin} = 0$; at this instant the switch is turned off. The threshold voltage V_T to trigger the close of SW is chosen to be slightly less than the peak voltage across C_{in} after a TENG charge while SW is off. Recall that the value of C_{in} is selected to draw maximal energy from the TENG with a fixed capacitor.

The energy transfer from the TENG to the load R can be divided into 4 phases (Fig. 2b).

- Phase 1: Energy flows from the TENG to C_{in} . During this phase, the switch SW is open, so that C_{in} is the only load for the TENG and its voltage quickly rises toward the maximal value.
- Phase 2: Energy flows from C_{in} to L, C_{out} and R. This phase starts as C_{in} 's voltage reaches the threshold value V_T . After that the switch SW is closed, allowing the energy in C_{in} to be transferred to L, C_{out} and R.

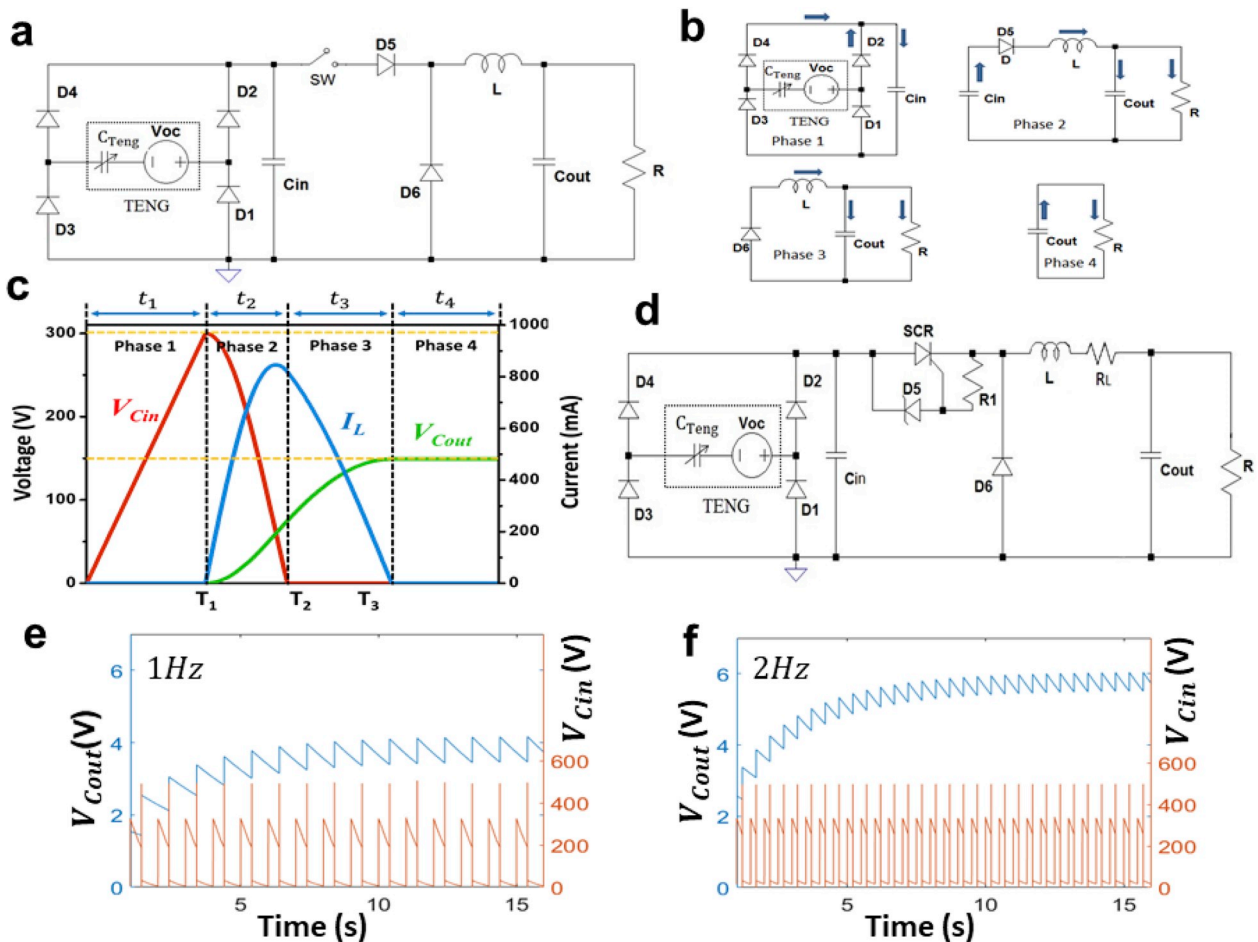


Fig. 2. a) An ideal buck converter topology for PMS. b) Four phases of energy transfer from TENG to the load; c) Simulation of four phases of energy flow. d) The complete circuit diagram of the proposed PMS. e),f) Simulated V_{Cin} and V_{Cout} .

This phase ends when the voltage across C_{in} decreases to 0 and C_{in} is completely discharged. During this phase, all energy in C_{in} is transferred to L , C_{out} and R .

- Phase 3: Energy flows from L to C_{out} and R . At the beginning of this phase, the diode $D6$ starts to conduct, which locks the voltage across C_{in} and its current to 0. The inductor L transfers its energy to C_{out} and R , with its current decreasing. This phase ends when L 's current decreases to 0, which means that all the energy in L is transferred to C_{out} and R . At the end of this phase, the diode $D6$ stops conducting.
- Phase 4: Energy flows from C_{out} to R . During this phase, all other elements are not conducting.

The 4 phases of energy transfer can be illustrated with the circuit diagram in Fig. 2b. The energy transfer during the 4 phases can also be demonstrated with the capacitor voltage and inductor current responses in Fig. 2c, assuming a linear increase of $V_{C_{in}}$ during Phase 1 and an ideal diode with 0 forward voltage. For clear demonstration of the process, the response is based on $C_{in} = 1$ nF, $C_{out} = 4$ nF, $L = 100$ μ H, $R = \infty$ and $V_{C_{out}}(0) = 0$. In realistic applications, C_{out} has much greater value than C_{in} . Typically, C_{in} is about 1 nF, C_{out} is above 20 μ F, then the duration of Phase 2 would be much shorter than that of Phase 3, making it hard to recognize the details in Phase 2.

During Phase 1, assume $V_{C_{in}}$ increases linearly from 0, and the threshold voltage for SW to close is $V_T = 300$ V. The precise function of $V_{C_{in}}$, which depends on the TENG device and is generally hard to express, does not affect the other 3 phases, as long as it increases monotonically toward V_T . During Phase 2 and Phase 3, the networks are simple RLC circuits, and the responses can be explicitly expressed as sinusoidal functions. In particular, during Phase 2,

$$I_L(t+T_1) = (V_{C_{in}}(T_1) - V_{C_{out}}(T_1)) \sqrt{\frac{C_{out}C_{in}}{L(C_{out} + C_{in})}} \sin\left(t \sqrt{\frac{C_{out} + C_{in}}{LC_{out}C_{in}}}\right), \quad (1)$$

$$V_{C_{in}}(t+T_1) = (V_{C_{in}}(T_1) - V_{C_{out}}(T_1)) \left(\frac{C_{out}}{C_{out} + C_{in}}\right) \left(\cos\left(t \sqrt{\frac{C_{out} + C_{in}}{LC_{out}C_{in}}}\right) - 1\right) + V_{C_{in}}(T_1) \quad (2)$$

$$V_{C_{out}}(t+T_1) = (V_{C_{in}}(T_1) - V_{C_{out}}(T_1)) \left(\frac{C_{in}}{C_{out} + C_{in}}\right) \left(1 - \cos\left(t \sqrt{\frac{C_{out} + C_{in}}{LC_{out}C_{in}}}\right)\right) + V_{C_{out}}(T_1) \quad (3)$$

The duration of Phase 2, t_2 , can be computed by setting $V_{C_{in}}(t_2 + T_1) = 0$, which gives,

$$t_2 = \sqrt{\frac{LC_{out}C_{in}}{C_{out} + C_{in}}} \cos^{-1}\left(1 - \frac{V_{C_{in}}(T_1)(C_{in} + C_{out})}{C_{out}(V_{C_{in}}(T_1) - V_{C_{out}}(T_1))}\right) \quad (4)$$

The values of $I_L(T_2) = I_L(t_2 + T_1)$ and $V_{C_{out}}(T_2) = V_{C_{out}}(t_2 + T_1)$ can be obtained by substitution,

$$I_L(T_2) = \sqrt{\frac{2V_{C_{in}}(T_1)(V_{C_{in}}(T_1) - V_{C_{out}}(T_1))C_{in}}{L} - \frac{(C_{in} + C_{out})V_{C_{in}}^2(T_1)C_{in}^2}{LC_{in}C_{out}}}, \quad (5)$$

$$V_{C_{out}}(T_2) = \frac{C_{in}V_{C_{in}}(T_1)}{C_{out}} + V_{C_{out}}(T_1) \quad (6)$$

During Phase 3,

$$I_L(t+T_2) = -\left(\sqrt{(I_L(T_2))^2 + \frac{C_{out}}{L}(V_{C_{out}}(T_2))^2}\right) \sin\left(\frac{t}{\sqrt{LC_{out}}} - \tan^{-1}\left(\frac{I_L(T_2)}{V_{C_{out}}(T_2)} \sqrt{\frac{L}{C_{out}}}\right)\right) \quad (7)$$

$$V_{C_{out}}(t+T_2) = \left(\sqrt{\frac{L}{C_{out}}(I_L(T_2))^2 + (V_{C_{out}}(T_2))^2}\right) \sin\left(\frac{t}{\sqrt{LC_{out}}} + \tan^{-1}\left(\frac{V_{C_{out}}(T_2)}{I_L(T_2)} \sqrt{\frac{C_{out}}{L}}\right)\right) \quad (8)$$

The duration of Phase 3, t_3 , can be computed by setting $I_L(t_3 + T_2) = 0$, which gives,

$$t_3 = \sqrt{LC_{out}} \tan^{-1}\left(\frac{I_L(T_2)}{V_{C_{out}}(T_2)} \sqrt{\frac{L}{C_{out}}}\right) \quad (9)$$

Using the identity $\tan^{-1}x + \tan^{-1}\frac{1}{x} = \frac{\pi}{2}$ yields

$$V_{C_{out}}(T_3) = V_{C_{out}}(t_3 + T_2) = \sqrt{\frac{L}{C_{out}}(I_L(T_2))^2 + (V_{C_{out}}(T_2))^2} \quad (10)$$

Further simplification after substituting $I_L(T_2)$ and $V_{C_{out}}(T_2)$, noting $V_{C_{in}}(T_1) = V_T$, the triggering voltage,

$$V_{C_{out}}(T_3) = \sqrt{\frac{C_{in}}{C_{out}} V_T^2 + V_{C_{out}}^2(T_1)} \quad (11)$$

At T_3 , the energy transfer from C_{in} to C_{out} is complete. As a result, the increment of energy stored in C_{out} during Phase 2 and Phase 3 is

$$\frac{1}{2}C_{out}V_{C_{out}}^2(T_3) - \frac{1}{2}C_{out}V_{C_{out}}^2(T_1) = \frac{1}{2}C_{out} \left(\frac{C_{in}}{C_{out}} V_T^2 + V_{C_{out}}^2(T_1)\right) - \frac{1}{2}C_{out}V_{C_{out}}^2(T_1) = \frac{1}{2}C_{in}V_T^2, \quad (12)$$

exactly equal to the energy drawn from the TENG by C_{in} after Phase 1, which verifies the lossless energy transfer from C_{in} to C_{out} under ideal assumptions. In Fig. 2c, $V_{C_{in}}(T_1) = V_T = 300$ V, $V_{C_{out}}(T_1) = 0$, at the beginning of Phase 2, and $V_{C_{out}}(T_3) = 150$ V at the end of Phase 3, where $C_{in} = 1$ nF, $C_{out} = 4$ nF, are used to generate the responses. If R is not infinite, $V_{C_{out}}$ will be decreasing during Phase 1 and Phase 4.

2.4. Practical implementation of the switch

In existing literature on PMS for TENGs, e.g. Ref. [25], the switches are implemented with MOSFETs and some logic devices which determine when to turn the switch on or off. Since a MOSFET needs a driver for its turn on and turn off, and both the driver and logic devices need a steady power supply of at least a few volts, the existing PMS cannot operate independently without additional power sources, such as a battery.

In this work, this challenge will be addressed by employing discrete semiconductor devices for the implementation of switches instead of using integrated driver and logic circuits. To be specific, a silicon-controlled rectifier (SCR) and a Zener diode will be used together to realize the switch's operation. The complete circuit for the proposed PMS is shown in Fig. 2d.

Here is a description of how the SCR and the Zener diode $D5$ implement the function of the switch SW in Fig. 2a. As the voltage across C_{in} exceeds the breakdown voltage of Zener diode $D5 + V_{C_{out}}$, $D5$ starts to reverse conduct, injecting current to the gate of the SCR and triggering it to conduct (like the close of a switch), with the SCR voltage instantly decreasing to 0, and starts Phase 2, during which $V_{C_{in}}$ decreases to nearly 0. At this instant, Phase 2 ends, $D6$ becomes forward biased and starts Phase 3. The forward conduction of $D6$ locks the voltage across C_{in} at around 0 and keeps the current through C_{in} and the SCR at 0, which is equivalent to turning off the switch and getting ready for the next TENG charge. It should be noted that R_1 between the cathode and the gate of the SCR is a shunt resistor which is used to minimize the possibility of premature SCR triggering via Zener diode's leakage current. In this configuration, the breakdown voltage of the Zener diode $+ V_{C_{out}}$ is equivalent to the trigger voltage V_T in the ideal buck converter topology. Since $V_{C_{out}}$ increases from 0 to a few volts during the transient period, V_T

also slightly increases by a few volts.

Fig. 2e and f shows some LTSpice simulation results as a proof of the concept. The blue sawtooth curve is $V_{C_{out}}$ and the orange pulsed curve is $V_{C_{in}}$. The parameters used for simulation are $C_{in} = 680$ pF, $L = 3.3$ mH, $RL = 2.5$ Ω , $C_{out} = 47$ μ F, $R = 248$ k Ω , $R_1 = 10$ k Ω . The SCR is EC103M1 and D6 is MUR460. The break down voltage of the Zener diode is 490V. The TENG frequency is 1 Hz in Figure 2e and 2Hz in Fig. 2f.

The figures show the increase of the output voltage $V_{C_{out}}$ to a steady state after about 16 s. The output voltage increases with the TENG frequency. The average output voltage at steady state is about 3.7 V at 1 Hz and 5.48V at 2 Hz. The peak to peak value for $V_{C_{out}}$ at steady state (the width of the sawtooth) can be reduced by increasing C_{out} , which increases the time for $V_{C_{out}}$ to reach a steady state.

Comparison of the output power and the total energy drawn by C_{in} in 1 s reveals some power loss in the PMS. For the case with 2 Hz rate of TENG charging, the steady state output voltage is about 5.48V, corresponding to an output power of 121 μ W. The peak voltage across C_{in} at steady state is 493V. The power drawn by the input capacitor C_{in} in 1 s is $\frac{1}{2}C_{in}V_{C_{in}}^2 \times f = \frac{1}{2} \times 680 \times 10^{-12} \times 493^2 \times 2W = 165.3$ μ W. The efficiency of power transfer from C_{in} to C_{out} is about 73.3% at a 2 Hz TENG frequency. The simulation software provides the power loss by the main circuit elements at steady state: $p(SCR) = 20$ μ W, $p(D6) = 16.3$ μ W, $p(RL) = 7.7$ μ W. In the next section, we will investigate the cause of power loss and how to minimize it by selecting appropriate circuit parts.

3. Power loss analysis and parameter optimization for maximum efficiency

The energy transfer should be lossless if ideal circuit elements are used. With a non-ideal diode, SCR and inductor, power loss in these devices is unavoidable. Therefore, each of the circuit elements should be

carefully chosen to minimize the power loss, considering the low power generated by a TENG. It turns out that there is a conflict between power loss reduction and element size reduction. To get some ideas about how to choose circuit elements, detailed analysis via LTSpice simulation will be conducted in this section to examine the power loss in each element. The simulation results will be generated based on the circuit in Fig. 2d.

3.1. Power loss in the SCR and relationship with inductance value

A practical SCR takes a few microseconds to fully turn on (when voltage decreases to nearly 0). Most power loss in the SCR occurs during its turn on interval. While the voltage response during the turn on interval does not vary much, the current depends on the inductance value. During this interval, the SCR current (which is the same as the inductor current) increases as power is transferred from C_{in} to the inductor. For a larger inductance value, the current increases at a slower rate, keeping the current at a lower value during the turn on of the SCR, yielding less power loss. This relationship is demonstrated with the simulation results in Fig. 3a and Fig. 3b, where a 1 mH inductor is used to generate Fig. 3a and a 15 mH inductor is used for Fig. 3b. The SCR model is EC103M1, the diode is MUR460 and $RL = 5\Omega$. With a 1 mH inductor, the SCR's peak power is about 10 W, averaged 56 μ W over a TENG charge period; with a 15 mH inductor, the peak power is 1.6W, averaged 17 μ W.

The above simulation results show that the power loss in SCR is closely related to the inductance value. To reduce the power loss in SCR, we may need to increase the inductance value and choose the SCR in the market with the fastest turn on time. However, increasing the inductance would generally increase the size of the inductor and R_L , the equivalent series resistance (ESR), which also incurs power loss.

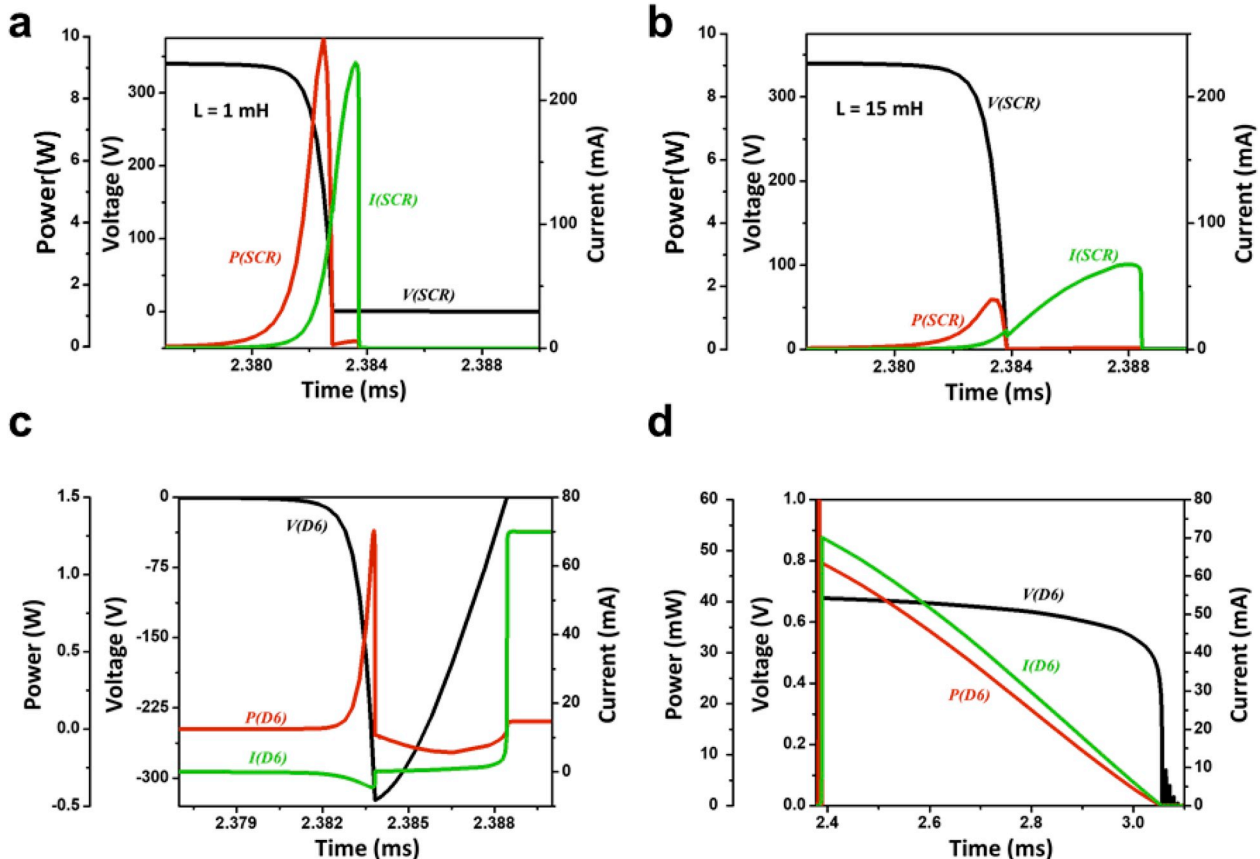


Fig. 3. Analysis of power loss in the switching devices via simulation. a),b) power loss in the SCR. c) d) power loss in the diode.

3.2. Power loss in the diode

For an ideal diode, the current is 0 during Phase 2 when power is transferred from C_{in} to the inductor. For a non-ideal diode, there will be some leakage current when it is reverse biased. Fig. 3c shows the voltage, the current and the power of the diode during Phase 2. It has some positive power during the turn on of SCR and some negative power between the fully on of SCR and its off when $V(C_{in})$ reaches 0. The positive energy and the negative energy are both around a few hundred nano Joules and nearly cancelled.

The power loss on the diode during the forward conducting interval in Phase 3 is more significant as demonstrated in Fig. 3d. For a particular diode model, MUR460, the power loss is around 16.3 μJ during Phase 3. This diode is selected because of the low forward voltage and low leakage current, as compared with other products of the same reverse voltage rating. For a forward current below 0.1 A, the forward voltage across the diode is below 0.7 V. Other models have higher forward voltage and consume more power.

The above analysis provides some general guidelines for choosing circuit parts for a practical implementation. First of all, due to TENG's high voltage output, most of the circuit elements, including the diode bridge, C_{in} , SCR, Zener diode, D6 are subject to at least a few hundred

volts. In the experimental circuit, all the parts have at least a 600 V voltage rating. Apart from satisfying the voltage rating, the SCR is selected as EC103M1 for fast turn on; the diode D6 is selected as MUR460 for its low forward voltage, low leakage current and fast recovery time. Several inductors of different inductance and ESR have been tested in the experiment, including (2.2 mH, 1.7 Ω), (3.3 mH, 1.428 Ω), (3.3 mH, 2.5 Ω), (10 mH, 3.394 Ω), (15 mH, 4.912 Ω). The one with 3.3 mH and 2.5 Ω is used on the prototype (Fig. 4a) for its size and the conversion efficiency.

4. Results and discussion

A prototype circuit for the PMS was constructed for a contact separation mode TENG, as seen in Fig. 4a, where the TENG device is the yellow object at the right hand side and the PMS prototype is at the left hand side. Comparison with a US quarter shows the size of the PMS circuit. The TENG device is activated by finger tapping. Fig. 4b shows the TENG device's charge and open circuit voltage at 3.3 Hz tapping.

The first element in the PMS to be selected is C_{in} based on the output response to a capacitive load. To choose C_{in} that draws maximal energy from the TENG after 1 finger tapping, the value of C_{in} is varied in a range and the peak output voltage is measured. Fig. 4c shows the peak voltage,

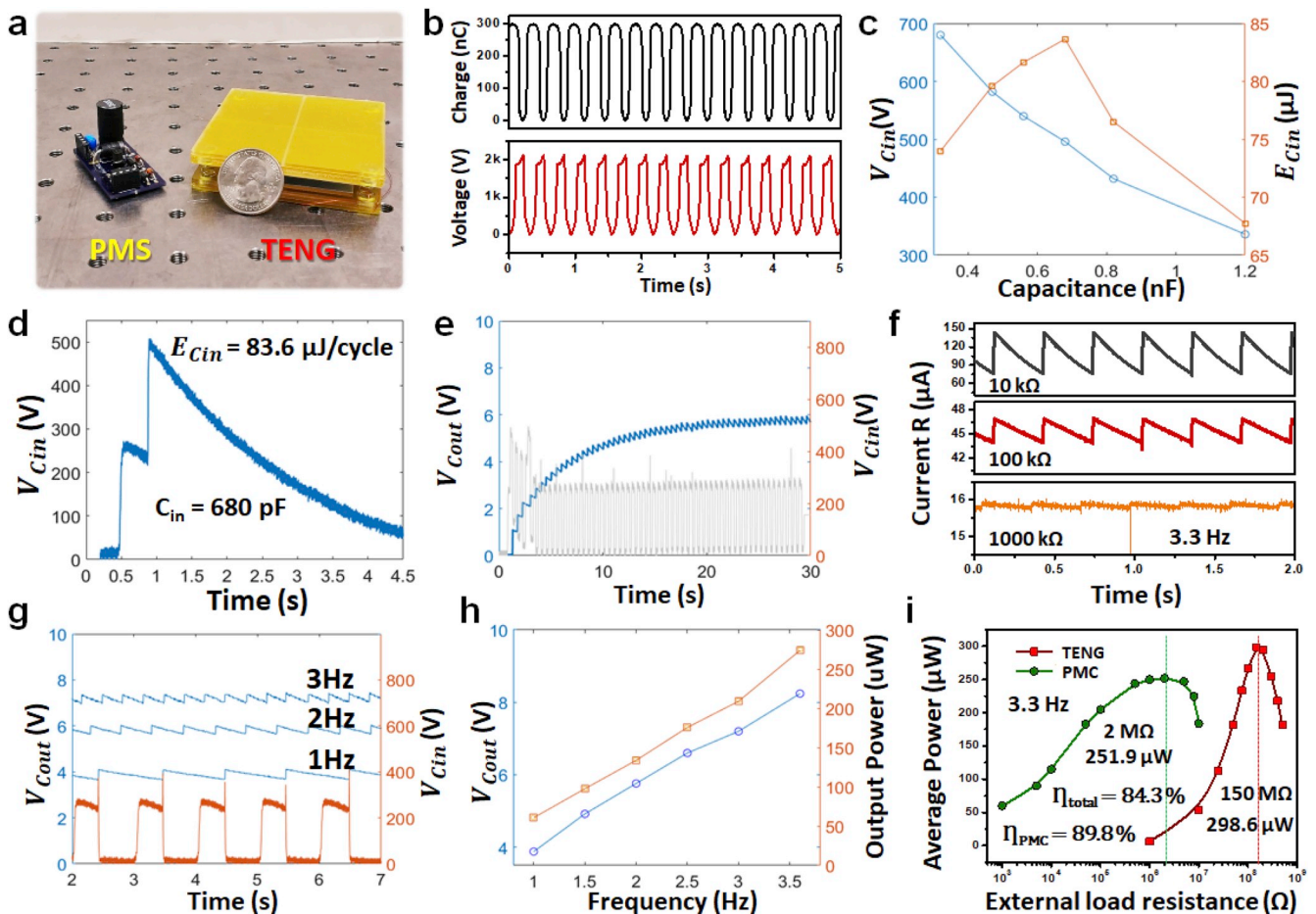


Fig. 4. a) Photograph of the PMS prototype, with the TENG and a US quarter. b) TENG's charge and output voltage. c) Peak voltage and energy transferred to C_{in} after one cycle of TENG charge, vs C_{in} capacitance. d) Response of V_{Cin} to one cycle of TENG charge under the optimal C_{in} . e) Output response of PMS measured from experiment, under 2 Hz TENG frequency, 248 k Ω load. f) Load resistor current at steady state for different values of R. g) Output voltage at steady state for different frequency. h) Dependence of average output voltage and power on TENG frequency. i) Output power of TENG and PMS vs load resistance, efficiency of PMS and overall conversion efficiency.

the energy stored in C_{in} as the capacitance is varied.

The value of C_{in} that draws maximal energy after one finger tapping is 680 pF. The voltage response across C_{in} at this value is plotted in Fig. 4d, where the first peak is caused by contact and the second peak caused by separation. The decrease after each peak is due to the leakage current in the diode bridge and the capacitor itself. The peak voltage is 496 V, corresponding to 83.6 μ J energy stored in C_{in} . This voltage value imposes a minimal voltage rating for the main elements in the PMS including the diode bridge, the SCR, and the diode D6. For the Zener diode, the breakdown voltage is chosen as 494 V, a little below the peak voltage 496 V, to ensure that the Zener diode is triggered after each tapping.

Several inductors have been tested for output performance. The one used on the PCB circuit in Fig. 4a is 3.3 mH with 2.5 Ω ESR. The capacitor at the output side C_{out} is 47 μ F. Experiments have been conducted under different values of load resistance R and tapping frequency.

Fig. 4e shows the transient response of $V_{C_{out}}$ (blue curve) at a 2 Hz tapping frequency. The load resistance is 248 k Ω . The voltage increases from 0 to a little below 6V after 20 s. The gray curve is $V_{C_{in}}$, where each pulse corresponds to one cycle of contact and separation. These voltage responses are very similar to the simulation results in Fig. 2f.

Fig. 4f shows the measured current through the load R for 3 different values of resistance, at a 3.3 Hz tapping frequency. As R is increased, the current ripple is reduced.

Fig. 4g shows the output voltage across R under 3 different tapping frequencies, when $R = 248$ k Ω . The pulsed curve at the bottom is the voltage across C_{in} under a 1 Hz tapping frequency, where the first rising edge is due to contact, the second rising edge due to separation, and the falling from the peak to the floor due to complete energy transfer from C_{in} to the inductor, which occurs in a few microseconds. The transfer of energy from the inductor to the output capacitor C_{out} is reflected by each sharp rise of $V_{C_{out}}$. The transfer of energy from C_{in} to C_{out} is accomplished within less than 1 ms and the detail cannot be seen in these oscilloscope waveforms.

It should be noted that the output voltage and current waveforms at steady state in Fig. 4f and g are a periodic sawtooth, as predicted in the simulation results in Fig. 2e and f. The voltage across C_{in} measured in experiment (orange pulse in Fig. 4g) is also very similar to the pulsed voltage in Fig. 2e and f. These results indicate that the PMS has achieved the intended energy flow strategy as designed for the circuit in Fig. 2d. Recall that the recent work [25] employs a similar buck converter topology, where a MOSFET and a comparator are used to implement a switch. The output voltages in Ref. [25] have similar ripples but are more irregular.

The dependence of output voltage and power on the tapping frequency is plotted in Fig. 4h, where R is fixed at 248 k Ω . The blue curve shows that the output voltage increases nearly linearly with the tapping frequency.

The overall output regulation performance and efficiency of the PMS is summarized in Fig. 4i, as compared with the output power of the TENG without using a PMS, all at a 3.3 Hz tapping frequency. The red curve shows the maximized effective output power when the TENG device is directly connected to a load resistor, where the load resistance is varied from 1 M Ω to 500 M Ω . It should be mentioned that we used the method in Ref. [29], which takes into account the air breakdown effect, to measure the effective output power without using PMS. The effective output power measured by this method is less than the value by some previous methods, e.g., in Ref. [26]. The maximized effective output power without using the PMS is 298.6 μ W, which is reached when $R = 150$ M Ω . The green curve shows the output power with the PMS, where the load resistance is varied from 1 k Ω to 10 M Ω . The maximum output power is 251.9 μ W, which is achieved when $R = 2$ M Ω . The measured power delivered to C_{in} under the same load is 280.5 μ W. The maximal efficiency of power transfer from C_{in} to the load is computed as 89.8%. The overall energy conversion efficiency of the PMS is computed as 84.3% by comparing the maximum output power with the PMS (251.9

μ W) and the maximum output power without the PMS (298.6 μ W). Similar energy conversion analysis was conducted in Ref. [25], which shows a total efficiency of 80.3% achieved by the buck converter based PMS.

A comparison of the two curves in Fig. 4i demonstrates a significant boost of output power for a wide range of load resistance below 10 M Ω . At 20 k Ω (1% of 2 M Ω), the output power is about 55% of the maximum value, at 2 k Ω (0.1% of 2 M Ω), the output power is about 30% of the maximum value. Similar conclusions can be drawn for the PMS in Ref. [25] which achieves maximum output power at 1 M Ω . At 10 k Ω , the output power is reduced to 11% of the maximum power.

5. Conclusions

A fully functional power management system is developed in this work for converting the pulse-like output of a TENG to steady voltage that can be used to supply power for conventional electronics and sensors. The PMS does not use any integrated circuits such as MOSFET drivers or comparators which may require an additional power supply other than TENG devices. The power management is achieved with a simple circuit topology consisting of only discrete semiconductor devices and an inductor. Experiment with a prototype circuit and a contact separation mode TENG verifies the effectiveness of the PMS. The TENG technology and the self-driven PMS presented in this work will provide a practical solution to self-powered systems. Future research will be conducted to further improve the output power and efficiency, and to reduce the size of the PMS.

Credit author statement

William Harmon: Design of circuit topology for PMS, Simulation, analysis, experiment, original draft, review, editing.

David Bamgboje: Optimization of circuit design and components for PMS, simulation, experiment, review, editing.

Hengyu Guo: TENG manufacturing, Experiment, PMS performance evaluation, Figure composition, review, editing.

Tingshu Hu: Project conceptualization and management, original draft, editing.

Zhong Lin Wang: Project conceptualization, team organization, funding acquisition.

Declaration of competing interest

The authors declare that they have no known competing financial interests or personal relationships that could have appeared to influence the work reported in this paper.

References

- [1] Z.L. Wang, J. Song, *Science* 312 (2006) 242.
- [2] F.-R. Fan, Z.-Q. Tian, Z. Lin Wang, *Nano Energy* 2 (2012) 328.
- [3] Z.L. Wang, *Sci. Am.* 298 (2008) 82.
- [4] F.R. Fan, L. Lin, G. Zhu, W. Wu, R. Zhang, Z.L. Wang, *Nano Lett.* 6 (2012) 3109.
- [5] S. Wang, L. Lin, Z.L. Wang, *Nano Lett.* 12 (2012) 6339.
- [6] Z.L. Wang, *Faraday Discuss* 176 (2014) 447.
- [7] H.-J. Yoon, R. Hanjun, S.-W. Kim, *Nano Energy* 51 (2018) 270.
- [8] S. Chandrasekaran, C. Bowen, J. Roscow, Y. Zhang, D.K. Dang, E.J. Kim, R.D. K. Misra, L. Deng, J.S. Chung, S.H. Hur, *Phys. Rep.* 792 (2019) 1.
- [9] Y. Zi, H. Guo, Z. Wen, M.H. Yeh, C. Hu, Z.L. Wang, *ACS Nano* 10 (2016) 4797.
- [10] Z.L. Wang, J. Chen, L. Lin, *Energy Environ. Sci.* 8 (2015) 2250.
- [11] T. Cheng, Q. Gao, Z.L. Wang, *Adv. Mater. Technol.* 4 (2019) 1800588.
- [12] Z. Zhang, K. Du, X. Chen, C. Xue, K. Wang, *Nano Energy* 53 (2018) 108.
- [13] X. Hou, J. Zhu, J. Qian, X. Niu, J. He, J. Mu, W. Geng, C. Xue, X. Chou, *ACS Appl. Mater. Interfaces* 10 (2018) 43661.
- [14] X.S. Zhang, M. Han, B. Kim, J.F. Bao, J. Brugger, H. Zhang, *Nano Energy* 47 (2018) 410.
- [15] B. Chen, Y. Yang, Z.L. Wang, *Adv. Energy Mater.* 8 (2018) 1702649.
- [16] Z. Wen, H. Guo, Y. Zi, M.H. Yeh, X. Wang, J. Deng, J. Wang, S. Li, C. Hu, L. Zhu, Z. L. Wang, *ACS Nano* 10 (2016) 6526.
- [17] Z.L. Wang, T. Jiang, L. Xu, *Nano Energy* 39 (2017) 9.
- [18] U. Khan, S.W. Kim, *ACS Nano* 10 (2016) 6429.

- [19] G. Cheng, Z.-H. Lin, L. Lin, Z.-L. Du, Z.L. Wang, ACS Nano 7 (8) (2013) 7383–7391.
- [20] Y. Zi, H. Guo, J. Wang, Z. Wen, S. Li, C. Hu, Z.L. Wang, Nano Energy 31 (2017) 302.
- [21] H. Qin, G. Cheng, Y. Zi, G. Gu, B. Zhang, W. Shang, F. Yang, J. Yang, Z. Du, Z. L. Wang, Adv. Funct. Mater. 28 (51) (2018) 1805216.
- [22] H. Qin, G. Gu, W. Shang, H. Luo, W. Zhang, P. Cui, B. Zhang, J. Guo, G. Cheng, Z. Du, Nano Energy 68 (2020) 104372.
- [23] F. Yang, L. Zhao, W. Shang, H. Qin, S. Wang, X. Jiang, G. Cheng, Z. Du, Nano Energy 46 (2018) 220–228.
- [24] G. Cheng, H. Zheng, F. Yang, L. Zhao, M. Zheng, J. Yang, H. Qin, Z. Du, Z.L. Wang, Nano Energy 44 (2018) 208–216.
- [25] F. Xi, Y. Pang, W. Li, T. Jiang, L. Zhang, T. Guo, G. Liu, C. Zhang, Z.L. Wang, Nano Energy 37 (2017) 168.
- [26] S. Niu, X. Wang, F. Yi, Y.S. Zhou, Z.L. Wang, Nat. Commun. 6 (1) (2015) 1–8.
- [27] X. Cheng, L. Miao, Y. Song, Z. Su, H. Chen, X. Chen, J. Zhang, H. Zhang, Nano Energy 38 (2017) 438.
- [28] S. Niu, Z.L. Wang, Nano Energy 14 (2015) 161.
- [29] Y. Zi, C. Wu, W. Ding, Z.L. Wang, Adv. Funct. Mater. 27 (2017) 1700049.



William Harmon received the B.Sc. and M.Sc. degrees in electrical engineering in 2010 and 2016 respectively and is working towards a Ph.D. degree in electrical engineering in the Department of Electrical and Computer Engineering, University of Massachusetts Lowell, MA, USA. He has worked professionally in the commercial power electronics industry and is currently working as an electrical engineer at Raytheon. His research interests include power conversion and power management systems for triboelectric nanogenerators.



David Bamgboje received the B.Sc. degree in electrical engineering from Obafemi Awolowo University, Nigeria, in 2012, the M.Sc. degree in electrical engineering from University of Ibadan, Nigeria, in 2016, and the Ph.D. degree from the University of Massachusetts Lowell, USA, in 2019. He is currently an adjunct professor in the Department of Electrical and Computer Engineering, University of Massachusetts Lowell, MA, USA. His research interests include high-efficiency power converters, LED driving systems and power management systems for nanogenerators.



Hengyu Guo received his B. S. and Ph.D. degree in Applied Physics from Chongqing University, China. Now he is a post-doctoral fellow in Georgia institute of technology, Zhong Lin Wang' group. His current research interest is triboelectric nanogenerator based energy and sensor systems.



Tingshu Hu received the B.S. and M.S. degrees in electrical engineering from Shanghai Jiao Tong University, Shanghai, China, in 1985 and 1988, respectively, and the Ph.D. degree in electrical engineering from the University of Virginia, Charlottesville, VA, USA, in 2001. She was a Postdoctoral Researcher with the University of Virginia and the University of California, Santa Barbara, USA. In January 2005, she joined the Faculty of Electrical and Computer Engineering, University of Massachusetts Lowell, Lowell, MA, USA, where she is currently a Professor. Her research interests include nonlinear systems theory, optimization, robust control theory, battery modeling and evaluation, control applications in power electronics and power management systems for nanogenerators.



Zhong Lin Wang received his Ph.D. from Arizona State University in physics. He now is the Hightower Chair in Materials Science and Engineering, Regents' Professor, Engineering Distinguished Professor and Director, Center for Nanostructure Characterization, at Georgia Tech. Dr. Wang has made original and innovative contributions to the synthesis, discovery, characterization and understanding of fundamental physical properties of oxide nanobelts and nanowires, as well as applications of nanowires in energy sciences, electronics, optoelectronics and biological science. His discovery and breakthroughs in developing nanogenerators established the principle and technological road map for harvesting mechanical energy from environment and biological systems for powering personal electronics. His research on self-powered nanosystems has inspired the worldwide effort in academia and industry for studying energy for micro-nano-systems, which is now a distinct disciplinary in energy research and future sensor networks. He coined and pioneered the field of piezotronics and piezophotonics by introducing piezoelectric potential gated charge transport process in fabricating new electronic and optoelectronic devices. Details can be found at: <http://www.nanoscience.gatech.edu>.